Secondary growth and photoluminescence from erbium implanted silica nanowires

A. Shalav,[a] T. H. Kim, and R. G. Elliman
Department of Electronic Materials Engineering, Research School of Physics and Engineering, The Australian National University, Canberra ACT 0200, Australia

(Received 27 September 2009; accepted 9 January 2010; published online 25 February 2010)

Gold-catalyzed silica nanowires were grown using vapor from the active oxidation of the silicon substrate and then implanted with erbium and annealed. During prolonged annealing at 1100 °C, where the concentration of vapor-phase reactants is sufficient to support nanowire growth, the erbium rich precipitates act as catalysts for the growth of a second generation of nanowires. These secondary nanowires increase in photoluminescence as they grow, suggesting that a fraction of the optically active erbium is incorporated into the growing wire. The resulting luminescent nanostructures have a very large surface-to-volume fraction and are well suited for optical-sensing applications. © *2010 American Institute of Physics*. [doi:10.1063/1.3309774]

Silica nanowires (NWs) are optically transparent, resistant to laser damage and chemically stable making them suitable hosts for optical dopants, particularly for optical based sensing applications. Although much work has been done on the intrinsic luminescence of silica NWs, attempts to functionalize them with optical dopants have only recently been investigated.[1–4] A recent study by Sekhar *et al.*[3] showed that optically active nanostructures could be fabricated by ion-implanting silica NWs with Er ions or by using Er as a catalyst for NW growth. In both cases the Er is incorporated within the silica NW as an optically active dopant that exhibits characteristic photoluminescence (PL) emission.

Dense arrays of amorphous substoichiometric silica (SiO_x) NWs can be produced by metal-induced vapor-liquid-solid (VLS) processes using a variety of methods.[5] One of the simplest of these involves the controlled annealing of a Si substrate at higher temperatures and low oxygen partial pressures to produce the vapor source of Si in the form of SiO.[6,7] Typically, a thin metal film (~10 nm) is deposited on Si and annealed at temperatures close to 1100 °C in a N_2 or Ar ambient containing residual O_2 at 3–5 ppm. At these temperatures, and O_2 concentrations, active oxidation of the silicon substrate occurs.[8,9] This reaction produces volatile SiO vapor, via the reaction $2Si+O_2 \rightarrow 2SiO$, most likely via adsorbed reaction Si/SiO_x intermediates.[10] Liquid metal-rich nanoparticles formed on the surface on the Si substrate by islanding of the metal film act as catalyst sites for silica NW growth. The metal almost certainly also enhances the reactive oxidation of Si to produce SiO vapor.[11] NWs grown using this method typically have diameters from tens of nanometers to a few hundred nanometers, with typical lengths of hundreds of micrometers and even up to a few millimeters.

In this study, the morphology and PL from ErO^- implanted SiO_x NWs is investigated as a function of annealing temperature and time. The results show that very high surface-area, optically active nanostructures can be produced by an appropriate choice of the implantation and annealing conditions. Such nanostructures are of particular interest for sensing applications where dopants can be used to detect adsorbates.[12,13]

Primary SiO_x NWs were grown on (100) Si substrates by first coating the wafers with a 10 nm evaporated Au thin-film and then annealing in a N_2 [100 SCCM (SCCM denotes cubic centimeter per at STP)] ambient for one hour at 1100 °C. The resulting NWs were then implanted with 30 keV ErO^- ions to low (1×10^{15} cm^{-2}), medium (1×10^{16} cm^{-2}), and high (2×10^{16} cm^{-2}) fluences as schematically illustrated in Fig. 1(a). The implanted samples were then sequentially annealed at increasing temperatures, ranging from 600 to 1100 °C for one hour in a N_2 (100 SCCM) ambient, and for extended periods (60–140 min) at 1100 °C. The characteristic $^4I_{13/2} \rightarrow {}^4I_{15/2}$ PL emission of the Er implanted NW's was measured at room temperature after each subsequent anneal up to 1100 °C using the 488 nm line of an argon ion laser as the excitation source. The emission spectra were obtained using standard lock-in techniques utilizing a liquid N_2 cooled Ge detector attached to a computer controlled Triax 320 monochromator.

Primary NWs had diameters in the range 500–1000 nm and lengths greater than 10 μm, as shown in Fig. 1(b), and their dimensions and morphology were unaffected by the ion-implantation process. Typical PL spectra from ErO^- implanted samples annealed at 900 °C are shown in Fig. 2. These spectra exhibit two distinct peaks, at around 1535 and 1547 nm, and are typical of the emission from Er^{3+} ions in silica. The form of the emission was invariant for samples implanted to different fluences and annealed at different tem-

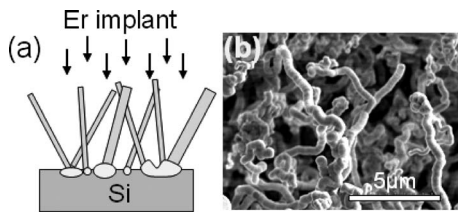

FIG. 1. (a) Schematic illustration showing implantation of primary NWs. (b) Typical SEM image of (unimplanted) primary NWs.

[a]Electronic mail: avi.shalav@anu.edu.au. Tel.: +61 2 612 51015.

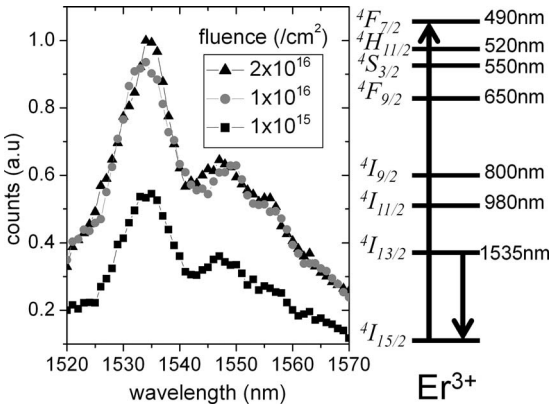

FIG. 2. Emission spectra after annealing at 900 °C for each fluence investigated. Also, on the right hand side, the energy level diagram for trivalent Er showing excitation (up arrow) and measured emission (down arrow).

peratures but the emission intensity has a strong dependence on annealing temperature as shown in Fig. 3.

For temperatures up to 900 °C the emission is observed to increase with increasing temperature, consistent with increasing optical activation of the Er and a reduction in nonradiative decay processes due to the annealing of implantation damage.[14] However, at higher temperatures the intensity is observed to decrease with increasing temperature. Similar behavior has previously been reported for bulk silica samples implanted with Er where the reduction was shown to result from Er precipitation within the silica which results in optical deactivation and concentration quenching effects.[14] Transmission electron microscopy (TEM) analysis of the present samples also shows the presence of Er-rich precipitates for samples annealed at temperatures above 900 °C. However, in this case the precipitates appear on the surface of the silica NWs, as shown in Fig. 4. The temperature dependence reported in Fig. 3 can therefore be understood in terms of the activation and precipitation of Er in silica.

Below 1000 °C, the passive oxidation of Si dominates the reaction between Si and O_2 and no SiO vapor is produced. Er-rich precipitates are therefore expected to remain on the silica NW surface and to play no further role in NW growth. However, at temperatures above 1000 °C, active oxidation is again dominant and SiO produced from the substrate can be adsorbed by the precipitated Er-rich nanoparticles. In this regime, such nanoparticles can act as effective catalyst particles for secondary NW growth as illustrated in Fig. 5. Significantly, the secondary NWs are smaller in diameter, have relatively short lengths, and exhibit a tapered form.

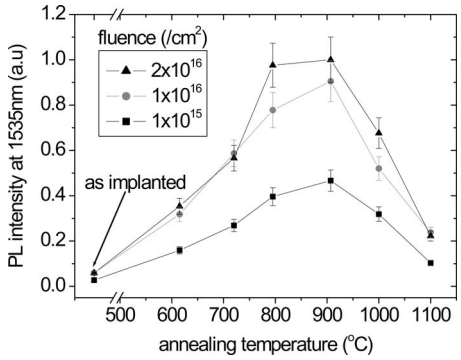

FIG. 3. 1535 nm peak PL intensity measurements for the Er implanted NW samples after subsequent annealing for one hour in N_2 at increasing temperatures up to 1100 °C.

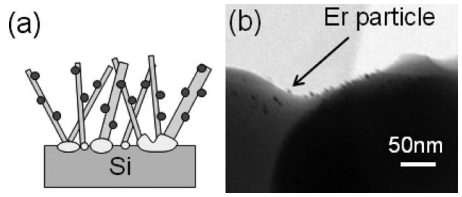

FIG. 4. (a) A schematic representation of precipitation and (b) a TEM image of precipitated Er-rich nanoparticles on a SiO_x NW annealed for 1 h at T < 1000 °C.

In order to study the secondary growth process and its influence on the Er PL emission, sequentially annealed samples were subjected to additional annealing at 1100 °C and their morphology and PL emission measured as a function of time. Samples grown in this regime exhibit a complex morphology that depends on the annealing time and implant fluence as summarized in Fig. 6. The luminescence intensity also shows a strong dependence on annealing time and, as seen in Fig. 6, can be correlated with the changes in nanostructure morphology. This suggests that optically active Er is incorporated within the secondary NWs as they grow, an effect that is analogous to the situation observed during the growth of primary NWs using Er as a catalyst.[3]

The morphology of the secondary NWs is particularly interesting and clearly results from the size and density of the Er-rich catalyst particles and the mode of growth. The melting point of Er metal is 1522 °C and it has no obvious compounds (oxides, silicides, etc) with melting points below 1100 °C. This suggests that the precipitated Er-rich particles on the primary NWs are solid and that secondary NW growth occurs by a vapor-solid-solid (VSS) mechanism.[15,16] VSS growth rates are typically 10–100 times slower than the VLS mechanism and can be attributed to slower precursor decomposition and slower diffusion through the solid catalyst.[16] This slow longitudinal growth of the secondary NWs would explain their short length and their tapered form as significant lateral growth of the NWs is expected at these temperatures due to adsorption of the vapor precursor onto the side walls of the growing NWs.

Figures 6(iv)–6(vi) and Figs. 7(a) and 7(b) show scanning electron microscopy (SEM) images for samples implanted with different Er fluences after additional annealing at 1100 °C. Comparing these images shows that the low fluence sample, although showing nucleation processes, does

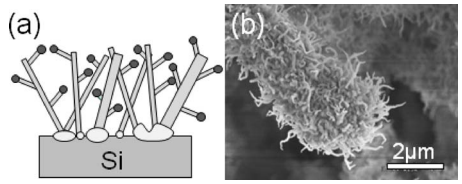

FIG. 5. (Color online) (a) A schematic representation of secondary growth and (b) a SEM image of secondary NW growth on a primary NW.

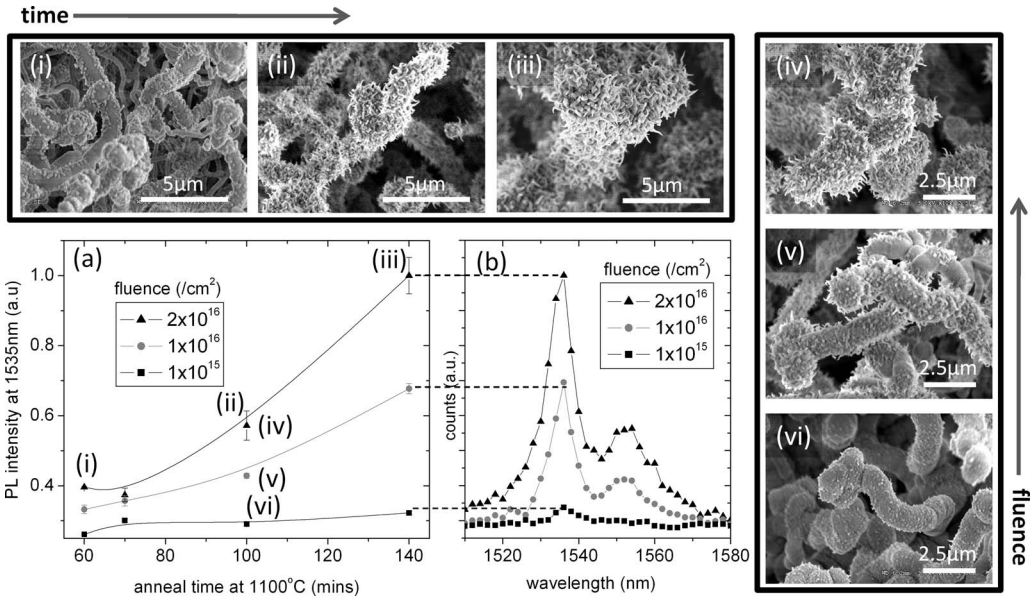

FIG. 6. (a) Peak (1535 nm) PL as a function of annealing time at 1100 °C. (b) PL spectra for the Er implanted NW samples after additional annealing for 140 min in N_2 at 1100 °C. SEM images (i–iii) show the evolution of the secondary NW growth as a function of time for the high fluence implanted sample, with corresponding PL emission labeled (i–iii) in (a). SEM images (iv–vi) show the morphologies of the high, medium and low fluence implanted samples, respectively, annealed at 1100 °C for 100 min, with corresponding PL emission labeled (iv–vi) in (a).

not exhibit homogeneous NW growth. This suggests that the limited amount of Er available in this case is insufficient to produce functional catalyst particles. In contrast, the high fluence sample shows well-defined tapered secondary NW growth as illustrated in Figs. 7(b)–7(d).

In summary, we have studied the morphology and PL emission of ErO^- implanted SiO_x NWs as a function of annealing temperature and time and shown that very high surface-area, optically active nanostructures can be produced by appropriate choice of implantation and annealing conditions. The PL emission intensity was shown to increase with increasing temperature for temperatures up to 900 °C, due to an increase in the optically active Er fraction, before decreasing with increasing temperature at higher temperatures due to Er precipitation. During prolonged anneals at temperatures above 1000 °C the precipitated Er-rich particles were shown to act as catalysts for the growth of a second generation of NWs. The morphology of these secondary NWs is dependent on the implanted ErO^- fluence, annealing temperature and time. High fluences and long anneal times resulted in short tapered NWs and is likely to be the consequence of the competition between slow longitudinal growth and lateral growth of the NWs caused by adsorption of the volatile reactants. The evolution of the secondary NW structures was correlated with an increase in the PL emission from Er suggesting that optically active Er is incorporated within the growing secondary NWs.

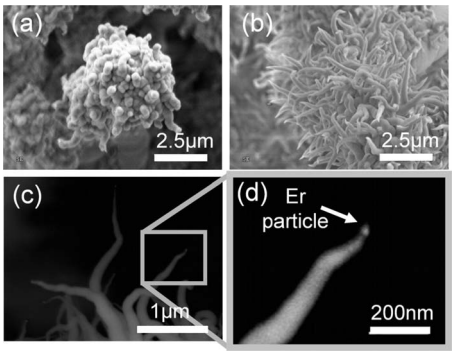

FIG. 7. SEM images showing secondary NW growth after annealing at 1100 °C (>300 mins) for (a) low and (b) high fluence Er implanted samples. (c) and (d) Backscattered electron images of the secondary NWs grown on the high Er implanted sample.

The authors are thankful to Dr. K. Belay for the preparation of the Er implantion into the SiO_x NWs and D. Llwellyn for his assistance with TEM analysis. A.S. acknowledges funding from the Australian Research Council (ARC).

[1]X. T. Zhang, Z. Liu, C. Wong, S. Hark, N. Ke, and S. Wong, J. Phys. Chem. C **111**, 4083 (2007).
[2]R. G. Elliman, A. R. Wilkinson, T. H. Kim, P. K. Sekhar, and S. Bhansali, J. Appl. Phys. **103**, 104304 (2008).
[3]P. K. Sekhar, A. R. Wilkinson, R. G. Elliman, T. H. Kim, and S. Bhansali, J. Phys. Chem. C **112**, 20109 (2008).
[4]R. G. Elliman, A. R. Wilkinson, T. H. Kim, P. K. Sekhar, and S. Bhansali, Nucl. Instrum. Methods Phys. Res. B **266**, 1362 (2008).
[5]C. N. R. Rao, F. L. Deepak, G. Gundiah, and A. Govindaraj, Prog. Solid State Chem. **31**, 5 (2003).
[6]A. S. Ferlauto, S. Oliveira, E. E. Silva, R. Magalhaes-Paniago, L. O. Ladeira, and R. G. Lacerda, J. Nanosci. Nanotechnol. **6**, 791 (2006).
[7]D. Bahloul-Hourlier and P. Perrot, J. Phase Equilib. Diffus. **28**, 150 (2007).
[8]J. J. Lander and J. Morrison, J. Appl. Phys. **33**, 2089 (1962).
[9]C. Gelain, A. Cassuto, and P. Legoff, Oxid. Met. **3**, 139 (1971).
[10]T. Engel, Surf. Sci. Rep. **18**, 93 (1993).
[11]A. Cros, J. Derrien, and F. Salvan, Surf. Sci. **110**, 471 (1981).
[12]M. S. Hu, H. L. Chen, C. H. Shen, L. S. Hong, B. R. Huang, K. H. Chen, and L. C. Chen, Nature Mater. **5**, 102 (2006).
[13]N. S. Ramgir, A. Zajac, P. K. Sekhar, L. Lee, T. A. Zhukov, and S. Bhansali, J. Phys. Chem. C **111**, 13981 (2007).
[14]A. Polman, J. Appl. Phys. **82**, 1 (1997).
[15]S. Kodambaka, J. Tersoff, M. C. Reuter, and F. M. Ross, Science **316**, 729 (2007).
[16]J. L. Lensch-Falk, E. R. Hemesath, D. E. Perea, and L. J. Lauhon, J. Mater. Chem. **19**, 849 (2009).